Inorg. Chem. **2007**, *46*, 4422–4429

Inorganic Chemistry
Article

Fluorescent Detection of Nitroaromatics and 2,3-Dimethyl-2,3-dinitrobutane (DMNB) by a Zinc Complex: (salophen)Zn

Meaghan E. Germain,[†] Thomas R. Vargo,[†] Peter G. Khalifah,[†] and Michael J. Knapp*[,†,‡]

Department of Chemistry and Program in Molecular and Cellular Biology, University of Massachusetts at Amherst, Amherst, Massachusetts 01003

Received October 19, 2006

Fluorescent sensors for the detection of chemical explosives are in great demand. It is shown herein that the fluorescence of Zn**L*** (H_2**L** = *N,N*′-phenylene-*bis*-(3,5-di-*tert*-butylsalicylideneimine)) is quenched in solution by nitroaromatics and 2,3-dimethyl-2,3-dinitrobutane (DMNB), chemical signatures of explosives. The relationship between the structure and fluorescence of Zn**L** is explored, and crystal structures of three forms of Zn**L**(base), (base = ethanol, tetrahydrofuran, pyridine) are reported, with the base = ethanol structure exhibiting a four-centered hydrogen bonding array. Solution structures are monitored by ^{1}H NMR and molecular weight determination, revealing a dimeric structure in poor donor solvents which converts to a monomeric structure in the presence of good donor solvents or added Lewis bases to form five-coordinate Zn**L**(base). Fluorescence wavelengths and quantum yields in solution are nearly insensitive to monomer–dimer interconversion, as well as to the identity of the Lewis base; in contrast, the emission wavelength in the solid state varies for different Zn**L**(base) due to π-stacking. Nitroaromatics and DMNB are moderately efficient quenchers of Zn**L***, with Stern–Volmer constants K_{SV} = 2–49 M^{-1} in acetonitrile solution.

Introduction

Chemical explosives detection is of much current interest for both defense and for the humanitarian purpose of clearing unexploded land mines.[1−7] Chemical explosives based upon trinitrotoluene also contain byproducts such as dinitrotoluene (DNT), making nitroaromatics important targets for explosives detection. While DNT has a moderate vapor pressure which may permit detection by canine teams, fluorescence-based detection methods are being developed to improve reliability. Examples of fluorescence-based sensors for DNT include conjugated polymers based on phenyleneethynylene,[7] polyacetylene,[1] and metalloles,[8] as nitroaromatics both bind tightly to these aromatic groups and quench the fluorescence of these easily oxidized fluorophores due to an electron-transfer process. Many plastic explosives do not contain nitroaromatics, however, making detection problematic for these compounds. Consequently, all commercially available plastic explosives are required by law to contain a high-vapor-pressure taggant, such as 2,3-dimethyl-2,3-dinitrobutane (DMNB), to facilitate detection by canine teams. Unfortunately, DMNB is challenging to detect by fluorescence quenching due to its low reduction potential, and we are aware of only a single report of fluorescence quenching by DMNB in which phenyleneethynylenes or polyphenylenes modified by π-donors exhibited moderately efficient quenching by DMNB.[3] Developing additional structures for the sensing of nitroaromatics and DMNB would facilitate multiplexing sensors[4,5] for improved reliability and sensitivity.

Salen complexes of diverse metals are widely used catalysts for organic transformations[9−11] such as epoxidations, aziridinations, and polymerizations, a well as attracting

* To whom correspondence should be addressed. Phone: 413-545-4001. E-mail: mknapp@chem.umass.edu.
[†] Department of Chemistry.
[‡] Program in Molecular and Cellular Biology.

(1) Liu, Y.; Mills, R. C.; Boncella, J. M.; Schanze, K. S. *Langmuir* **2001**, *17*, 7452−7455.
(2) Toal, S. J.; Trogler, W. C. *J. Mater. Chem.* **2006**, *16*, 2871−2883.
(3) Thomas, S. W.; Amara, J. P.; Bjork, R. E.; Swager, T. M. *Chem. Commun.* **2005**, 4572−4574.
(4) Albert, K. J.; Myrick, M. L.; Brown, S. B.; James, D. L.; Milanovich, F. P.; Walt, D. R. *Environ. Sci. Technol.* **2001**, *35*, 3193−3200.
(5) Moore, D. S. *Rev. Sci. Instrum.* **2004**, *75*, 2499−2512.
(6) Czarnik, A. W. *Nature* **1998**, *394*, 417−418.
(7) Yang, J. S.; Swager, T. M. *J. Am. Chem. Soc.* **1998**, *120*, 11864−11873.
(8) Sohn, H.; Sailor, M. J.; Magde, D.; Trogler, W. C. *J. Am. Chem. Soc.* **2003**, *125*, 3821−3830.
(9) Atwood, D. A.; Harvey, M. J. *Chem. Rev.* **2001**, *101*, 37−52.

10.1021/ic062012c CCC: $37.00
Published on Web 05/02/2007

Scheme 1

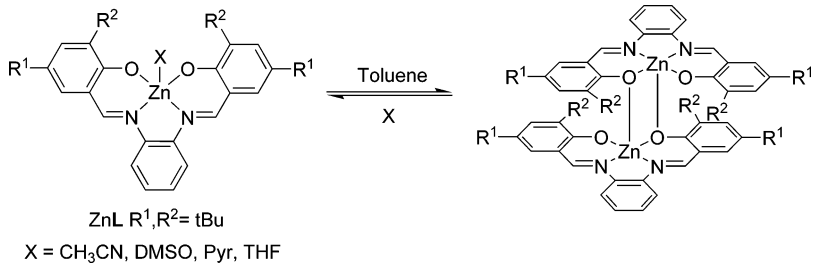

attention as building blocks for supramolecular chemistry.[12−14] Adding to their catalytic and structural properties, (Salen)-Zn[15] complexes have recently been shown to exhibit fluorescence properties similar to those of the well-known fluorophores based on (porphyrin)Zn,[16−18] suggesting that (salen)Zn and related structures may be useful for optical or sensory materials. Solution-phase emission quantum yields (ϕ_{em}) for (salen)Zn vary widely in response to molecular structure,[17] ranging from 6×10^{-3} to 0.74.[16,17,19] Energy transfer on the sub-nanosecond time scale was also shown within a supramolecular assembly of (salen)Zn and Re(I),[16] demonstrating that the excited-state of (salen)Zn participates in rapid photochemistry. Reports of fluorescence in the solid state[19,20] and thin films,[21] as well as electroluminescence from thin layers of (aldimine)Zn,[22,23] suggest that these complexes may hold promise as OLEDs, in addition to their potential sensory application.

In consideration of the reported fluorescence properties for (salen)Zn, we probed the relationship between structure and emission wavelength for Zn**L** (Scheme 1, H_2**L** = *N*,*N*′-phenylene-*bis*-(3,5-di-*tert*-butylsalicylideneimine), as well as testing the fluorescence quenching of this structure by nitroaromatics and DMNB. We herein report that Zn**L** undergoes moderately efficient fluorescence quenching in the solution phase by electron transfer with nitroaromatics and DMNB. While H_2**L** is a tetradentate ligand, the strong preference of Zn(II) for pentacoordination is evident from the observation that solid-state structures of (salen)Zn complexes are pentacoordinate, either due to the addition of a monodentate ligand, which is possible when the salicylaldehyde substituents R^1 and R^2 are large, or by formation of phenol-bridged dimers, when these substituents are small.[20,24−27] Solution NMR and molecular weight determinations are reported herein to establish a similar speciation between monomeric and dimeric structures (Scheme 1). The fluorescence properties of Zn**L** are not changed significantly by the monomer−dimer equilibrium or by the binding of a variety of Lewis bases to form monomeric Zn**L**(base). In contrast, X-ray crystallographically determined structures of three forms of Zn**L**(base) reveal that solid-state packing changes significantly with different Lewis bases, which leads to a large shift in the solid-state emission wavelength.

Experimental Methods

All chemicals were purchased from Aldrich and Fisher Scientific and used as received unless specified. Solvents were purchased from VWR scientific, dried, and distilled from CaH_2 (MeCN), Mg (EtOH), Na (Toluene), Na benzophenone (THF), or CaH_2 (CH_2Cl_2). Phenylenediamine was recrystallized from water and stored in an inert atmosphere glovebox until use. NMR solvents were purchased from Cambridge Isotope Laboratories and used as received. Elemental analyses (C, H, N) were performed at the University of Massachusetts microanalysis laboratory.

ZnL(base). To a flask of dry ethanol, *ortho*-phenylenediamine (0.5 mmol) and 3,5-di-*tert*-butyl salicylaldehyde (1 mmol) were added and refluxed overnight. The reaction mixture was filtered and a yellow solid, H_2**L** was collected. H_2**L** (0.5 mmol), was dissolved in ethanol with heat and a solution of $Zn(OAc)_2$ (0.5 mmol) in ethanol was added dropwise. The orange solution was refluxed for 2 h and cooled to room temperature. Bright orange crystals of Zn**L**(EtOH)·EtOH were collected and analyzed. Elemental analysis for $C_{40}H_{57}N_2O_4Zn$ cald (found): C 69.10 (69.02), H 8.28 (8.44), N 4.03 (3.96). ^{1}H NMR (CD_2Cl_2): δ 8.32 (bs, 2H imine), 7.37 (d 2H aromatic), δ 7.28 (bs 4H aromatic), δ 6.77 (bs 2H aromatic), 3.63 (q 4H CH_2 ethanol), 1.40 (bs, 18H *t*-butyl), 1.27 (s, 18H, *t*-butyl), 1.17 (t, 6H, CH_3 ethanol). Recrystallization of Zn**L**(EtOH)·(EtOH) from the respective solvents yielded yellow crystals of Zn**L**(py) or orange crystals of Zn**L**(THF).

X-ray crystallography. Data were collected on a Bruker-Nonius KappaCCD diffractometer utilizing Mo Kα radiation. Epoxy was

(10) Cohen, C. T.; Chu, T.; Coates, G. W. *J. Am. Chem. Soc.* **2005**, *127*, 10869−10878.
(11) Canali, L.; Sherrington, D. C. *Chem. Soc. Rev.* **1999**, *28*, 85−93.
(12) Sun, S. S.; Stern, C. L.; Nguyen, S. T.; Hupp, J. T. *J. Am. Chem. Soc.* **2004**, *126*, 6314−6326.
(13) Kleij, A. W.; Kuil, M.; Lutz, M.; Tooke, D. M.; Spek, A. L.; Kamer, P. C. J.; van Leeuwen, P. W. N. M.; Reek, J. N. H. *Inorg. Chim. Acta* **2006**, *359*, 1807−1814.
(14) Kleij, A. W.; Kuil, M.; Tooke, D. M.; Lutz, M.; Spek, A. L.; Reek, J. N. H. *Chem.-Eur. J.* **2005**, *11*, 4743−4750.
(15) We use Salen to indicate the generic class of salicylaldimine ligands formed by the Schiff base condensation of salicylaldehyde with a diamine. Salophen refers to the subset in which *ortho*-phenylenediamine is used as the diamine.
(16) Splan, K. E.; Massari, A. M.; Morris, G. A.; Sun, S. S.; Reina, E.; Nguyen, S. T.; Hupp, J. T. *Eur. J. Inorg. Chem.* **2003**, 2348−2351.
(17) Chang, K. H.; Huang, C. C.; Liu, Y. H.; Hu, Y. H.; Chou, P. T.; Lin, Y. C. *J. Chem. Soc., Dalton Trans.* **2004**, 1731−1738.
(18) Freeman, D. C.; White, C. E. *J. Am. Chem. Soc.* **1956**, *78*, 2678−2682.
(19) Mizukami, S.; Houjou, H.; Sugaya, K.; Koyama, E.; Tokuhisa, H.; Sasaki, T.; Kanesato, M. *Chem. Mater.* **2005**, *17*, 50−56.
(20) Mizukami, S.; Houjou, H.; Nagawa, Y.; Kanesato, M. *Chem. Commun.* **2003**, 1148−1149.
(21) Di Bella, S.; Leonardi, N.; Consiglio, G.; Sortino, S.; Fragala, I. *Eur. J. Inorg. Chem.* **2004**, 4561−4565.
(22) Hamada, Y.; Sano, T.; Fujita, M.; Fujii, T.; Nishio, Y.; Shibata, K. *Jpn. J. Appl. Phys. 2* **1993**, *32*, L511−L513.
(23) Sano, T.; Nishio, Y.; Hamada, Y.; Takahashi, H.; Usuki, T.; Shibata, K. *J. Mater. Chem.* **2000**, *10*, 157−161.
(24) Singer, A. L.; Atwood, D. A. *Inorg. Chim. Acta* **1998**, *277*, 157−162.
(25) Reglinski, J.; Morris, S.; Stevenson, D. E. *Polyhedron* **2002**, *21*, 2175−2182.
(26) Szlyk, E.; Wojtczak, A.; Surdykowski, A.; Gozdzikiewicz, M. *Inorg. Chim. Acta* **2005**, *358*, 467−475.
(27) Gallo, E.; Solari, E.; Re, N.; Floriani, C.; ChiesiVilla, A.; Rizzoli, C. *J. Am. Chem. Soc.* **1997**, *119*, 5144−5154.

Table 1. Crystallographic Data for Zn**L**(EtOH)·EtOH, Zn**L**(THF), and Zn**L**(py)

	Zn**L**(EtOH)·EtOH	Zn**L**(THF)	Zn**L**(py)
empirical formula	$C_{40}H_{58}N_2O_4Zn$	$C_{40}H_{54}N_2O_3Zn$	$C_{41}H_{51}N_3O_2Zn$
M (g mol^{-1})	696.25	676.22	683.22
cryst syst	monoclinic	triclinic	orthorhombic
space group	$P2_1/c$ (No. 14)	$P\bar{1}$ (No. 2)	$Pbcm$ (No. 57)
a (Å)	13.1292(3)	10.9600(4)	15.4018(2)
b (Å)	24.9288(5)	13.0670(5)	10.4556(1)
c (Å)	11.6353(2)	13.1540(5)	23.1113(3)
α (deg)	90	91.943(2)	90
β (deg)	91.4833(8)	104.094(2)	90
γ (deg)	90	92.054(2)	90
V (Å^3)	3806.9(1)	1824.2(1)	3721.73(9)
Z	4	2	4
temp (K)	125	120	120
ρ_{calc} (g/cm^3)	1.215	1.231	1.219
μ(Mo K$_a$) (mm^{-1})	0.686	0.712	0.697
F(000)	1496	724	1456
θ range (°)	3.7−27.5	3.7−25.7	3.7−27.5
reflns collected	16 596	11 682	8092
indep reflns	8682	6863	4354
obsd reflns [$I > 2\sigma$]	5432	5667	3685
R_{int}	0.0622	0.0413	0.0197
params refined	442	615	331
R1 (all, $>4\sigma$)	0.1014, 0.0477	0.0575, 0.0425	0.0429, 0.0327
wR2 (all, $>4\sigma$)	0.1168, 0.1018	0.1067, 0.096	0.0859, 0.0799
χ^2	1.020	1.054	1.046
$\Delta\rho$(min,max,av) (e/Å^3)	0.60, −0.38, 0.07	0.75, −0.80, 0.06	0.39, −0.49, 0.05

used to mount crystals on a thin glass fiber, which were cooled to ~125 K in the cold stream produced of an Oxford Cryosystems cooler. Scans were designed using the Bruker-Nonius Collect package,[28] while integration and scaling were done using the routines HKL2000 and Scalepak.[29] Structure solutions were obtained using the SIR software,[30,31] providing atomic coordinates for a refinement using SHELXL-97,[32] utilizing the interface and the additional utilities of WinGX.[33] In Zn**L**(THF) and Zn**L**(py), the data quality allowed hydrogens to be located from the difference map and freely refined with isotropic thermal parameters. This was not the case for Zn**L**(EtOH)·EtOH, where hydrogens could only be reasonably refined by constraining them to ideal geometries and performing a riding refinement with hydrogen thermal parameters fixed at a multiple of their bounded partner. Structures were validated using the functionality of PLATON.[34,35] Crystallographic data are summarized in Table 1.

Physical Characterization. Electrochemical measurements were performed on a BAS CV50W cyclic voltammeter using Fc/Fc^+ as an internal standard, 0.1 M tetrabutylammonium hexafluorophosphate as a supporting electrolyte, a Pt working electrode, a Pt auxiliary electrode, and Ag/AgCl as a reference electrode. ^{1}H NMR spectra were collected with a Bruker 400 MHz (400.13 MHz) spectrometer. Solution molecular weight determinations were measured by vapor pressure osmometry using a Wespro Vapro model 5520 calibrated with benzil.

NMR titration spectra were collected in CD_2Cl_2 (EtOH) or CD_3-CN (nitriquinoline). The titrations were monitored by chemical shift changes of the imine peak (~8.3 ppm). Titration of ethanol was performed at a 12 mM Zn**L** concentration with EtOH added via micropipet. Titration of nitroquinoline was performed in the same manner with a Zn**L** concentration of 8 mM; due to spectral overlap in the aromatic region, the nitroquinoline titration was not taken to completion.

Absorbance measurements were collected in a quartz cuvette with a 1 cm path length on a Hewlett-Packard 8453 UV−vis spectrophotometer. Quantum yield measurements were performed in a quartz, 1 cm path length cuvette, on a JASCO FP-6500 spectrofluorometer in acetonitrile, ethanol, pyridine, tetrahydrofuran, and toluene. Quinine sulfate in 0.1 M H_2SO_4, used as a standard (ϕ = 0.54),[36−38] was excited at 400 nm and the emission monitored at 450 nm. Solutions of Zn**L** were also excited at 400 nm and monitored at λ_{em} = 530−540 nm. The resulting fluorescence intensities were plotted against solution absorbances to generate a linear plot to calculate the quantum yield of Zn**L** in different solvent environments.[39]

Results and Discussion

Description of Structures. Crystals suitable for X-ray diffraction were obtained by recrystallizing Zn**L** from the respective solvents, and the structures determined at ~125 K. The structures of Zn**L**(base), base = THF, py, were previously determined at room temperature and reported;[24] however, those coordinates are not available through the Cambridge Structural Database. We collected these data in order to compare the intermolecular interactions in these solid lattices. As the metrical details for these two structures are available,[24] only the relationship between intermolecular interactions of these complexes and emission wavelength will be discussed.

The molecular structure of Zn**L**(EtOH)·EtOH revealed that the ethanol ligand to Zn(II) was hydrogen-bonded to the ethanol solvate (Figure 1). Bond lengths for the Zn**L** moiety are in line with similar compounds,[24−26] with Zn−O bonds of 1.9302(16) and 1.9586(16) Å, and Zn−N bonds of 2.0498(19) and 2.082(2) Å. The Zn(II) lies 0.291 Å above the plane defined by the N_2O_2 coordination shell of the salophen ligand, being distorted upward toward the axial ethanol. Similar distortions for base = THF (0.304 Å) and py (0.386 Å) are observed.[24] The Zn−base bond lengths for py, THF, and EtOH are 2.094, 2.178, and 2.161(2) Å, respectively.

Pentacoordinate Zn(II) can take a geometry ranging from square planar to trigonal bipyramidal. The geometry about Zn(II) was analyzed with the formalism in which internal angles are combined into a single parameter, τ, which ranges from 0 for square pyramidal to 1 for trigonal bipyramidal.[40] Zn**L**(py) is perfectly square pyramidal, τ = 0, while Zn**L**(EtOH) and Zn**L**(THF) are very nearly square pyramidal

(28) Mackay, S.; Gilmore, C. J.; Edwards, C.; Stewart, N.; Shankland, K. Bruker Nonius, MacScience Japan, University of Glasgow: Delft, The Netherlands, 1999.
(29) Otwinowski, Z.; Minor, W. In *Macromolecular Crystallography, Part A*; Academic Press: San Diego, 1997; Vol. 276, pp 307−326.
(30) Altomare, A.; Burla, M. C.; Camalli, M.; Cascarano, G. L.; Giacovazzo, C.; Guagliardi, A.; Moliterni, A. G. G.; Polidori, G.; Spagna, R. *J. Appl. Crystallogr.* **1999**, *32*, 115−119.
(31) Burla, M. C.; Camalli, M.; Carrozzini, B.; Cascarano, G. L.; Giacovazzo, C.; Polidori, G.; Spagna, R. *J. Appl. Crystallogr.* **2003**, *36*, 1103.
(32) Sheldrick, G. M. University of Gottingen: Gottingen, Germany, 1998.
(33) Farrugia, L. J. *J. Appl. Crystallogr.* **1999**, *32*, 837−838.
(34) Spek, A. L. *Acta Crystallogr., Sect. A* **1990**, *46*, C34.
(35) Spek, A. L. Utrecht University: Utecht, The Netherlands, 1998.
(36) Chen, Z. K.; Huang, W.; Wang, L. H.; Kang, E. T.; Chen, B. J.; Lee, C. S.; Lee, S. T. *Macromolecules* **2000**, *33*, 9015−9025.
(37) Demas, J. N.; Crosby, G. A. *J. Phys. Chem.* **1971**, *75*, 991-&.
(38) Melhuish, W. H. *J. Phys. Chem.* **1961**, *65*, 229-&.
(39) Williams, A. T. R.; Winfield, S. A.; Miller, J. N. *Analyst* **1983**, *108*, 1067−1071.
(40) Addison, A. W.; Rao, T. N.; Reedijk, J.; Vanrijn, J.; Verschoor, G. C. *J. Chem. Soc., Dalton Trans.* **1984**, 1349−1356.

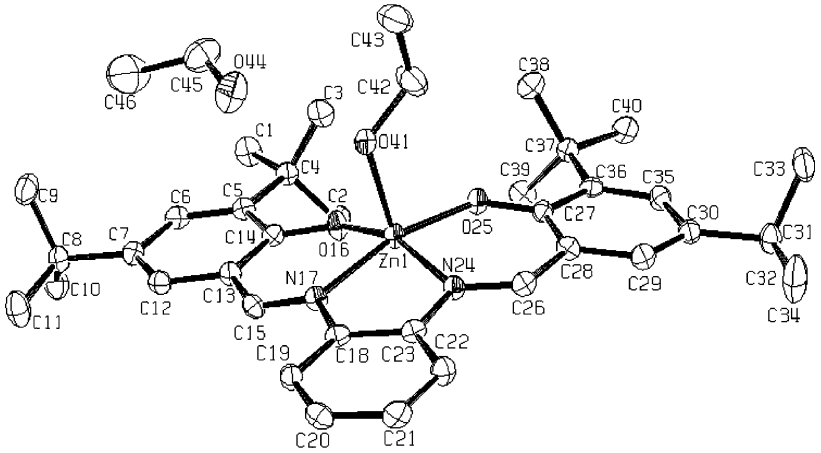

Figure 1. ORTEP of Zn**L**(EtOH)·EtOH. H-atoms omitted for clarity.

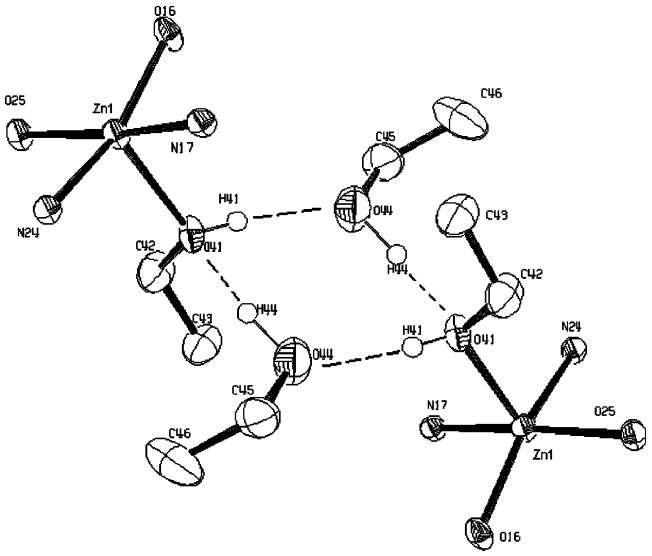

Figure 2. Hydrogen-bonding array in Zn**L**(EtOH)·EtOH. Select bond lengths (Å) and bond angles (deg): O41−H41, 0.79(3); O41−O44, 2.679; O44−O41, 2.963; O44−H44, 0.82; O41−H41−O44, 170; O44−H44−O41, 150.

with $\tau = 0.12$ and 0.14, respectively. A survey of the Cambridge Crystallographic Database failed to reveal any other examples of square pyramidal geometry in (salen)Zn complexes; however, several other (salen)Zn complexes with 3,5-di-*tert*-butyl salicylidene groups exhibit τ in the range 0.16−0.33.[17,24,26]

Inspection of the lattice for close contacts revealed the presence of a hydrogen-bonded array between the ethanols of two asymmetric units, forming a supramolecular dimer (Figure 2). This hydrogen bonded array is planar and homodromic, in which the directionality of hydrogen-bond donors follow a cyclic arrangement.[41,42] The bond distances for hydrogen-bond donors and acceptors are 2.679 Å for O41−O44 (O41 is the hydrogen-bond donor) and 2.963 Å for O44−O41 that are typical for moderate strength hydrogen bonds.[43] The X-ray structure was of sufficient quality to resolve the electron density of all hydrogens, with O41−H41 distances of 0.79(3) Å and O44−H44 distances of 0.82 Å observed. While one might anticipate that the O41−H41 bond should be lengthened from the combined effects of being a hydrogen-bond donor and a ligand to the Lewis-acidic Zn(II), it has been noted that X-ray structures are biased due to the polarization of the electron density in hydrogen-bonded pairs.[43] Therefore, the internuclear O−H distances are likely to be very close to the typical value of 0.9 Å for both O−H bonds.[43]

There is one prior report of a four-member hydrogen-bonded array involving ethanol coordinated to Zn(II) in interpenetrating (porphyrin)Zn complexes.[42] The present crystal structure is of higher quality by virtue of the minimal disorder from the smaller salophen ligands and thus gives better metrical details for the hydrogen-bonding array. As the strength of typical hydrogen bonds between neutral molecules is relatively weak($-\Delta H \approx 2-5$ kcal/mol),[44] the four-member hydrogen-bond array would stabilize the supramolecular dimer by less than 20 kcal/mol. The entropic cost of assembling the six molecules (4 EtOH and 2 Zn**L**) will likely exceed this enthalpic stabilization, however, and it is unlikely that such a dimer would form in solution. In fact, solution ^{1}H NMR in CD_2Cl_2 show the number of peaks anticipated for a C_s-symmetric Zn**L**, indicating that the dimer observed crystallographically is not present at detectible levels in solution (however, see the NMR data below).

The lattice packing for each of the three structures was inspected for intermolecular contacts. Figure 3 shows that π-stacking is present for both Zn**L**(THF) and Zn**L**(EtOH), but entirely absent for Zn**L**(py). In the THF and EtOH complexes, the diimine aryl ring of one Zn**L** stacks onto the imine groups of an adjacent Zn**L**, such that the angle between the N_2O_2 planes is 0°. The N_2O_2 planes are separated by 3.41 Å in Zn**L**(THF) and 3.44 Å in Zn**L**(EtOH), indicating close intermolecular contacts. On the other hand, the intermolecular interaction for Zn**L**(py) is predominantly between the diimine aryl ring and the C−H protons of

(41) Chacko, K. K.; Saenger, W. *J. Am. Chem. Soc.* **1981**, *103*, 1708−1715.
(42) Nakash, M.; Clyde-Watson, Z.; Feeder, N.; Teat, S. J.; Sanders, J. K. M. *Chem.-Eur. J* **2000**, *6*, 2112−2119.
(43) Steiner, T.; Saenger, W. *Acta Crystallogr., Sect. B* **1994**, *50*, 348−357.
(44) Perrin, C. L.; Nielson, J. B. *Annu. Rev. Phys. Chem.* **1997**, *48*, 511−544.

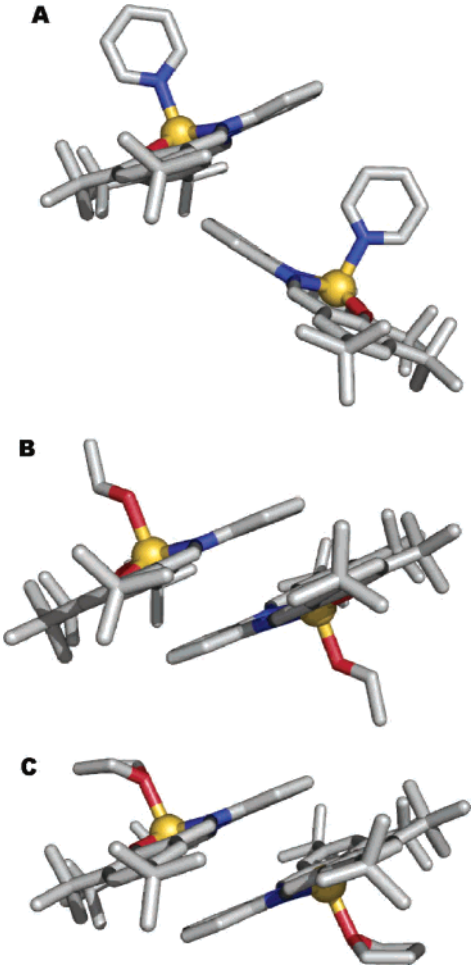

Figure 3. Ligand contacts and π-stacking within the lattice of Zn**L**(base). (A) Pyridine. (B) Ethanol. (C) Tetrahydrofuran.

coordinated pyridine. The angle between the N_2O_2 planes is 47°, indicating the absence of π-stacking.

Ligand Binding and Speciation. The tendency of (salen)-Zn complexes to crystallize as five-coordinate molecular units is well known in the literature, with a phenolate-bridged dimer and a Lewis-base coordinated monomer the dominant structural motifs.[20,24−26] The above crystal forms for Zn**L** arise from the binding of solvents that are good Lewis bases, consistent with the expectation that rapid ligand exchange for Zn**L** would lead to coordination of available bases. In the course of characterizing Zn**L** we noticed that the ^{1}H NMR spectra of Zn**L**(EtOH)·EtOH in CD_2Cl_2 exhibited the number of peaks expected for Zn**L** with effective C_s symmetry, indicating that the hydrogen-bonding network was lost (Figure 4). However, the breadth of the ^{1}H NMR linewidths suggested that a chemical exchange process occurred in solution. If the solution chemical exchange process were due to a monomer−dimer equilibrium, then the molecular mass for Zn**L** would change between a good donor solvent and a poor donor solvent.

Zn**L**(EtOH)·EtOH was dissolved in acetonitrile and toluene, and vapor pressure osmometry (VPO) was used to measure the solution molecular weight (MW_{obs}). As the VPO instrument was designed for use with aqueous solutions, solvents with vapor pressures comparable to water were

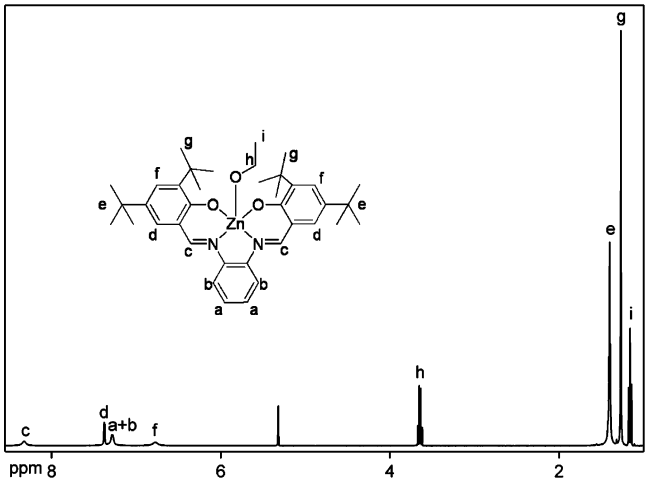

Figure 4. ^{1}H NMR of Zn**L**(EtOH)·EtOH in CD_2Cl_2.

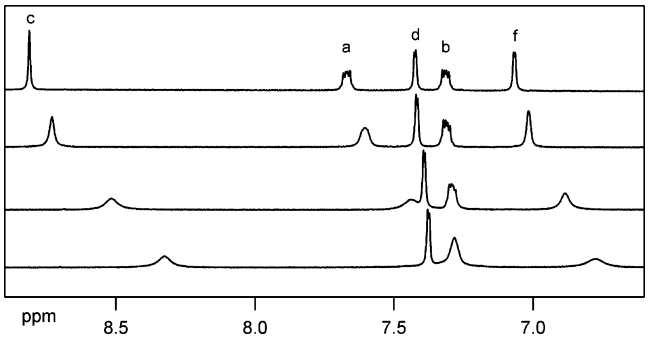

Figure 5. ^{1}H NMR titration of Zn**L**(EtOH)·EtOH (12 mM) in CD_2Cl_2. Total EtOH concentrations from bottom to top: 25, 71, 146, 370 mM. Peaks labeled as in Figure 4.

needed; the high vapor pressure of CH_2Cl_2 precluded its use. The MW_{obs} differed from 714 g/mol in acetonitrile to 1164 g/mol in toluene, compared with a true formula weight for Zn**L** of 602 g/mol and for Zn**L**(EtOH)·EtOH of 696 g/mol. Zn**L** exists largely as a monomeric species in acetonitrile, consistent with the good donor properties of this solvent which likely leads to the formation of Zn**L**(CH_3CN), whereas a dimeric structure dominates in toluene.

The dimeric species could be bridged by either the hydrogen bonds of the ethanol molecules or through a phenolate. As Zn**L**(py) lacks opportunities for hydrogen-bonding interactions and any dimeric species formed from this molecule would most likely be phenolate-bridged, Zn**L**(py) was also analyzed by VPO. The solution state molecular weight of Zn**L**(py) in toluene is 1195 g/mol, indicating that the dimeric structure of Zn**L** found in solution is likely bridged through phenolate bonding interactions. The broad NMR peaks in dichloromethane most likely reflect a dynamic monomer−dimer equilibrium.

To push the equilibrium to favor the monomeric species, a dichloromethane solution of ethanol (2.2 M) was titrated into a dichloromethane solution of Zn**L**(EtOH)·EtOH (12 mM), and the chemical shift of the imine proton was used to monitor speciation. The imine peak is initially observed at 8.324 ppm in CD_2Cl_2 and shifts to a value of 8.809 ppm at 370 mM ethanol concentrations, as shown in Figure 5. Additionally, the NMR peaks all narrow and sharpen at

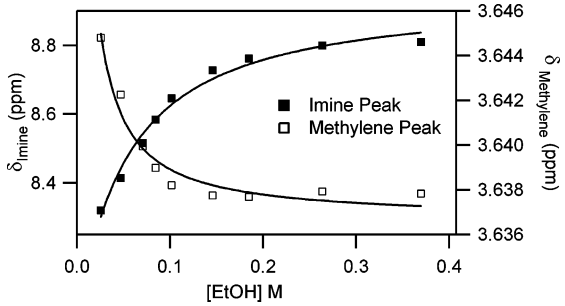

Figure 6. Ethanol titration of Zn**L** (12 mM) in dichloromethane (400 MHz NMR). See text for fitting details.

elevated ethanol concentrations, indicating that a single structure dominates under these conditions. The chemical shift of the imine peak was plotted as a function of total ethanol concentration, and the resulting saturation curve, shown in Figure 6, suggested a simple 1:1 binding model: Zn**L**(EtOH) ⇆ Zn**L** + EtOH.

This binding model leads to eq 1, in which δ_{obs} is the observed chemical shift, δ_i and δ_f are the initial and final chemical shift values, and K_D is the dissociation constant. The best fit curve resulted in the following parameters: $\delta_i = 8.012 \pm 0.09$ ppm, $\delta_f = 8.950 \pm 0.04$ ppm, $K_D = 0.049 \pm 0.014$ M. Likewise, the chemical shift of the methylene group of EtOH changed from 3.645 to 3.638 ppm upon addition of 370 mM EtOH. The methylene binding curve was fit using eq 1 to obtain $\delta_i = 3.661 \pm 0.009$ ppm, $\delta_f = 3.637 \pm 0.0005$ ppm, and $K_D = 0.0089 \pm 0.006$ M. This equilibrium constant is weaker than expected, as similar (salen)Zn complexes bind pyridines[14,16] or methanol[13] with an affinity of roughly 10^{-4} M. The apparent weakness of ethanol binding in this case may reflect the competitive nature of the equilibrium.

$$\delta_{obs} = \frac{\delta_f - \delta_i}{2[\text{EtOH}]}\{([\text{EtOH}] + [\text{Zn}\mathbf{L}] + K_D) - \sqrt{([\text{EtOH}] + [\text{Zn}\mathbf{L}] + K_D)^2 - 4[\text{EtOH}][\text{Zn}\mathbf{L}]}\} + \delta_i \quad (1)$$

The NMR titration and the solution molecular weight determination indicate that Zn**L** equilibrates between a monomeric and dimeric species in solution. The position of the equilibrium depends upon the availability of Lewis bases which can coordinate to Zn**L**, which in concert with the reported crystal structures indicates that good donor solvents are likely to form a Zn**L**(solvent) monomeric species. In dichloromethane, addition of ethanol pushed the equilibrium to favor the monomeric Zn**L** species. This monomer−dimer equilibrium was seen to also depend upon the bulk solvent, as a monomeric species was favored in the good donor solvent acetonitrile, whereas a dimeric structure was favored in toluene. This tendency of (salen)Zn to acquire an axial ligand has been used in supramolecular chemistry, such as in the energy-transfer work of Hupp and Nguyen[16] and the recent report of a bifunctional hydroformylation catalyst from the Reek group.[45]

(45) Kuil, M.; Goudriaan, P. E.; van Leeuwen, P. W. N. M.; Reek, J. N. H. *Chem. Commun.* **2006**, in press.

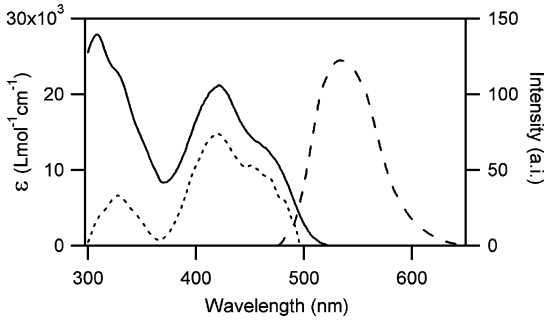

Figure 7. Electronic absorption (solid line), emission (dotted line), and excitation (dashed line) spectra of Zn**L**(EtOH)·EtOH in dichloromethane solution.

Table 2. Electronic Absorption, Emission, and Fluorescence Quantum Yield of Zn**L**

solvent	λ_{max} (abs)	λ_{max} (emiss)	ϕ_{em}
dichloromethane	424 nm	538 nm	0.30
toluene	424 nm	535 nm	0.35
acetonitrile	422 nm	538 nm	0.36
ethanol	422 nm	533 nm	0.43
pyridine	425 nm	535 nm	0.55
THF	422 nm	531 nm	0.59

Excited-State Redox Potential. A small number of reports indicated that (salen)Zn complexes exhibit fluorescence as both solids and solutions,[16−21] suggesting that they may be suitable for fluorescence-based sensing. Hupp, et al.[16] demonstrated that energy transfer was efficient for (salen)-Zn; however, the lack of visible absorption for many analytes, including nitroaromatics, makes energy transfer an unsuitable mechanism for detection. The excited-state redox properties of Zn**L** were estimated to determine its suitability for electron-transfer reactivity with nitro-containing molecules.

Absorption, excitation, and emission spectra of Zn**L** were measured in dichloromethane (Figure 7). The peak absorption at 424 nm (λ_{max}) exhibited a low-energy shoulder at ~450 nm. The emission maximum is 538 nm, with an excitation maximum of 424 nm. These are consistent with prior reports for salen-type ligands with aromatic diamines,[16,17] in which the fluorescent excited state was described as dominantly singlet in character.[16]

To test for the effects of coordinated base, Zn**L**(EtOH)·EtOH was dissolved in common solvents then filtered to ensure removal of any solids. The solvents ethanol, pyridine, and THF were shown to coordinate to Zn**L** to form the Zn**L**(solvent) complex by crystallography, and the finding that Zn**L** in acetonitrile forms a monomeric species indicates that acetonitrile is also likely to also coordinate. In these donor solvents, it is likely that Zn**L**(solvent) will be the dominant solution species. In each of these solvents, the absorption, emission, and excitation spectra were nearly superimposable with that of a dichloromethane solution (Table 2). This shows that the identity of the coordinated base affects neither the absorption nor emission properties to any significant extent.

Quantum yields for emission (ϕ_{em}) for the fluorescent excited state were also measured in different solvents to quantify any changes in the fluorescent excited state due to coordinated solvent or the monomer/dimer equilibration. In

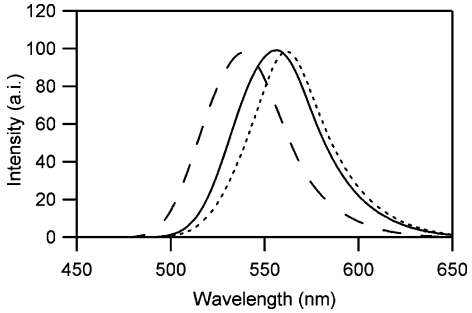

Figure 8. Emission spectra of Zn**L**(base) microcrystalline solids (dashed = py, solid = EtOH, dotted = THF).

Table 3. Electrochemistry of Zn**L** (1 mM) in Acetonitrile[a]

E_c	E_a	ΔE	$E_{1/2}$
0.430	0.315	0.115	0.373
0.633	0.538	0.095	0.586

[a] vs $Fc^{0/+}$, 0.1M TBA(PF_6)

each solvent tested, ϕ_{em} varied only modestly over the range 0.3−0.6, despite the significant variation in solvent properties over this series. It is clear that the fluorescent excited state is not overly sensitive to changes in axial ligand nor to changes in solvent composition.

Cyclic voltammetry of Zn**L**(EtOH)·EtOH (1 mM) in acetonitrile revealed two quasi-reversible redox processes at positive potential. The first oxidation process at $E_{1/2}$ = +0.373 V, Zn**L** → Zn**L**$^+$ + e$^-$, is likely localized on the phenolate ring of the salophen ligand. The second oxidation process may be a subsequent oxidation to form the dicationic species Zn**L**$^{2+}$; however, this will not be considered further.

The excited-state energy (E_{00}) was estimated from the intersection of the absorption and emission spectra at 492 nm, E_{00} = 2.52V. We estimate the uncertainty in this value at ±0.1 eV. The excited-state oxidation potential for Zn**L*** ($E_{(ZnL+/ZnL^*)}$) was estimated from E_{00} and the ground-state oxidation potential ($E_{(ZnL+/ZnL)}$) as −2.1 V using eq 2.

$$E_{(ZnL+/ZnL^*)} = E_{(ZnL+/ZnL)} - E_{00} = -2.1\ \text{V} \qquad (2)$$

Zn**L*** is a strongly reducing excited state, with a driving force sufficient to reduce many nitroaromatics, as well as DMNB.[46] This suggested that the excited state (Zn**L***) would be quenched by such compounds.

Solid-State Effects on Fluorescence. The color of the Zn**L**(base) solids depended on the coordinated base, leading us to also measure solid-state emission spectra (Figure 8). The maximum emission wavelength increased by 22 nm over the series (py < EtOH < THF). This trend may reflect the donor properties of the base, in which case solution properties would vary depending upon the Lewis basicity of the solvent, or on π-stacking within the lattice. As the emission and absorption spectra for Zn**L** did not vary in different solvents, we conclude that the differences observed in the solid state arise from intermolecular interactions, rather than from the properties of coordinated ligands.

(46) Measured redox potentials in V (vs $Fc^{+/0}$): 2,3-dimethyl-2,3-dinitrobutane (DMNB), −2.00; nitro-*m*-xylene (NX), −1.85; nitrotoluene (NT), −1.62; nitrobenzene (NB), −1.57; nitroquinoline (NQ), −1.38.

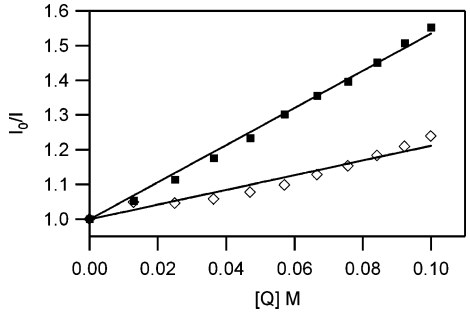

Figure 9. Quenching of Zn**L** (4.3μM) fluorescence by NT (■) or DMNB (◇) in acetonitrile.

Chart 1. Quencher Structures and Stern−Volmer Constants for Quenching Zn**L** in Acetonitrile

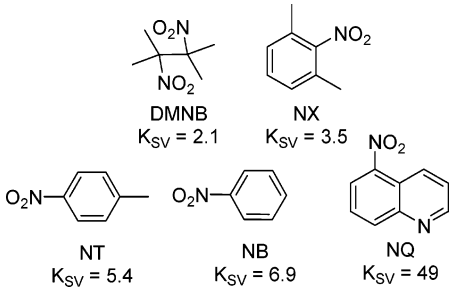

The packing within the solid state for the EtOH and THF structures revealed that salophen ligands adopted parallel planar structures, such that adjacent salophen ligands were $\pi-\pi$ stacked at a distance of 3.4 Å. In contrast, the salophen ligands within the py structure were not in the registry, adopting canted orientations with closest contacts between salophen ligand and the py ligand from an adjacent molecule. As π-stacking is known to cause red-shifts in emission spectra in other systems,[19] this is likely the origin of the red-shift in emission wavelength for Zn**L**(THF) and Zn**L**(EtOH) relative to Zn**L**(py).

Quenching by Nitroaromatics and DMNB. The strongly reducing nature of Zn**L*** prompted us to investigate fluorescence quenching by DMNB and nitroaromatics in CH_3CN solution. Titrating DMNB, nitro-*m*-xylene (NX), nitrotoluene (NT), nitrobenzene (NB), and nitroquinoline (NQ) quenched the fluorescence at 538 nm. Analysis of the normalized fluorescence intensity (I_0/I) as a function of increasing quencher concentration ([Q]) was well described by the Stern−Volmer equation, $I_0/I = 1 + K_{SV}[Q]$, for all titrants. Linear Stern−Volmer behavior is consistent with quenching that is dominated by a dynamic process, in which the titrant collides with Zn**L*** to quench the fluorescent excited state; the titrations of NT and DMNB are shown as examples in Figure 9.

The Stern−Volmer constants (K_{SV}) reflects the competition between bimolecular quenching and unimolecular fluorescence decay, with K_{SV} indicating the efficiency of quenching relative to the intrinsic fluorescent lifetime. Quenching efficiencies rage from 2.1 M^{-1} for DMNB to 49 M^{-1} for nitroquinoline (Chart 1). As the fluorescence lifetimes of related (salen)Zn are in the range of 1×10^{-9} s and our quenching efficiencies are roughly 5 M^{-1}, it is likely that the bimolecular quenching rates are in the range of 5×10^9

M^{-1} s^{-1}. Indirect comparisons of the quenching efficiency of Zn**L** to the polymeric metalloles of Sailor and Trogler[8] or the amplifying fluorescent polymers (AFPs) of Swager[3,7,47] and others[1] are possible with the caveat that those polymeric fluorophores are quenched by static mechanisms. Polymeric metalloles with a repeat length of about 10 units are highly efficient quenchers of nitroaromatics, with solution quenching efficiencies up to 1200 M^{-1} toward nitrobenzene.[8] However, the dominant interaction with nitroaromatics is proposed to be π-stacking with partial charge-transfer, which is not expected to be applicable to DMNB;[8] no report of metallole quenching by DMNB has appeared. AFPs are conjugated fluorescent polymers which show similar quenching efficiencies in solution toward nitroaromatics, with a similar reliance on π-stacking.[1,7,8,47] One report[3] of quenching efficiencies for DMNB toward thin-film AFPs are in the range of $K_{SV} = 3-20$ M^{-1}, which are up to 10-fold higher than the solution-phase (CH_3CN) quenching efficiency of DMNB toward Zn**L**.

The proposed quenching reaction is Zn**L*** + RNO_2 → $ZnL^+ + RNO_2^-$, in which the nitro compound accepts an electron from the excited state of Zn**L**. The driving force (ΔG) for this photoinduced electron-transfer reaction is favorable, based upon the redox potentials ($\Delta G = -nF(E_{(RNO_2/RNO_2^-)} - E_{(ZnL^*/ZnL^+)})$). In support of this electron-transfer mechanism is the linear relationship between ln K_{SV} and $E_{1/2}$ (Figure 10) for all quenchers except NQ. NQ exhibits a significantly higher quenching efficiency, suggesting that it may quench Zn**L*** by a static process that involves binding to the axial position of Zn**L**. Our attempts to quantify NQ binding to Zn**L** by ^{1}H NMR were unsuccessful due to the overlapping chemical shifts of Zn**L** and nitroquinoline (data not shown); however, the Zn**L** imine chemical shift changed from 7.979 to 7.757 ppm upon addition of 48 mM NQ, indicating that a weak binding interaction took place.

(47) Yang, J. S.; Swager, T. M. *J. Am. Chem. Soc.* **1998**, *120*, 5321−5322.

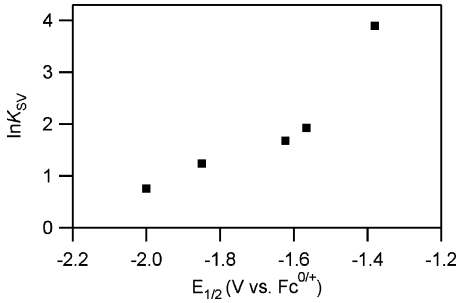

Figure 10. Quenching efficiency (K_{SV}) for each nitro compound with Zn**L** vs observed reduction potentials in acetonitrile.

Conclusions

The solution fluorescence of Zn**L** is quenched by nitroaromatics and DMNB with Stern−Volmer constants of $K_{SV} \approx 2-49$ M^{-1}. While there is much room for improvement in the response of Zn**L** toward DMNB, the salophen backbone provides a starting point for developing improved DMNB sensors. Zn**L** forms a dimeric structure in solution which converts to a monomeric structure by binding Lewis bases, as shown by ^{1}H NMR and solution molecular weight measurements. The fluorescence quantum yield in solution is nearly insensitive to axial ligand identity or dimerization. The emission spectra of Zn**L**(base) in the solid state varies due to π-stacking interactions, suggesting that the fluorescence properties of Zn**L** may be tunable in the solid state by environmental perturbations. We also report an aesthetically pleasing hydrogen-bonded array of four ethanol molecules which bridge two Zn**L** units into a supramolecular assembly.

Acknowledgment. We thank Robert Herbst for X-ray data collection and refinement. The X-ray Structural Characterization Laboratory is supported by the National Science Foundation (CHE-9974648).

Supporting Information Available: Crystallographic information files (CIF) and figures of Stern−Volmer quenching. This material is available free of charge via the Internet at http://pubs.acs.org.

IC062012C